Hindawi
Advances in Materials Science and Engineering
Volume 2018, Article ID 8651239, 14 pages
https://doi.org/10.1155/2018/8651239

Research Article

Strength Characteristics and the Reaction Mechanism of Stone Powder Cement Tailings Backfill

Jianhua Hu,[1] **Qifan Ren**,[2] **Quan Jiang**,[2] **Rugao Gao**,[1] **Long Zhang**,[2] **and Zhouquan Luo**[1]

[1]*Professor, School of Resources and Safety Engineering, Central South University, Changsha, Hunan 410081, China*
[2]*Research Assistant, School of Resources and Safety Engineering, Central South University, Changsha, Hunan 410081, China*

Correspondence should be addressed to Qifan Ren; qifanren@csu.edu.cn

Received 14 March 2018; Accepted 17 October 2018; Published 13 November 2018

Guest Editor: Syed W. Haider

Stone powder cement (SPC) is widely used as a novel cement substitute material in concrete for its good gelling performance and low cost. In order to reduce the backfilling cost and assess the potential of SPC backfilling materials, a series of experiments were conducted to analyze the strength and hydration reaction mechanism of stone powder cement tailings backfill (SPCTB). The analysis was based on SPC and tailings, which were used as the gelling agent and the aggregate, respectively. The results showed that the strength of the backfill was greatly reduced at an early stage and slightly reduced in the final stages. The stone powder content was less than 15%, which met the requirement of mining procedure. The addition of stone powder reduced the content of adsorbed water and capillary water in the early stages, while it increased in the middle stages. The SiO_2 contained in stone powder reacted with the hydration products at later stages, which is the reason why the growth of strength is rapid between the groups with the addition of stone powder. The addition of stone powder improved the microstructure of backfill and produced a denser three-dimensional (3D) network structure; however, the plane porosities of Groups A and B gradually increased with the increase in the content of stone powder. The cement powder mixed appropriately with the stone power could meet the strength requirement and reduce the cost of backfilling materials.

1. Introduction

When manufacturing crushed aggregate, the process creates a stone powder, which could be collected and used to produce SPC. The majority of particles of stone powder range from 1 μm to 100 μm, making them difficult to handle, transport, and recycle. The quantity of stone powder produced from crushed aggregate factories in China is approximately 10 million tons per year, most of which is dumped in soil. The disposal of stone powder is a major environmental problem, and therefore, there is a great interest to find solutions for its safe utilization [1]. Portland cement is used as a gelling agent in traditional backfill in mines, whereas the high cost of cement needs a suitable and sustainable low-cost substitute. In China, most of the mines are in mountainous areas surrounded by quarries where the stone powder is thrown out every year and causes a lot of environmental pollution [2]. However, it can be collected and utilized in backfill. Figure 1 shows a quarry.

Al-Kheetan et al. [3, 4] introduced crystalline material along with a curing compound in fresh concrete to protect and extend its service life and developed hydrophobic concrete by adding dual-crystalline admixture during the mixing stage. Choi et al. [1] examined the microstructure and strength of alkali-activated systems using stone powder sludge, which had some water content as a replacement material in alkali-activated mixtures that strengthened the concrete's ability to withstand extreme variable temperatures and loads. Compared to ordinary concrete, other properties, including early gain in compressive strength, durability, and high acid and fire resistance, make it an appealing construction material. Compressive strengths of four different natural pozzolans with the replacement level of 10–25% at various ages were studied [5]. The results

Figure 1: Quarry around the mine.

showed that, with the increase in natural pozzolans content, natural pozzolans replacements reduced the compressive strengths of concrete due to reduction in cement content in the mixture. However the compressive strength increases with age. Several investigations [6, 7] showed that the compressive strength of mortars with different cements and incorporating 10% silica fume was about 30–50% higher than that of plain cements after 28 days. The strength of silica fume mortars depends on the water to binder ratio of the mixture. The compressive strength of mortars containing 10% silica fume decreases with the decrease in the fineness of parent Portland cement. However, it is always higher than the strength of plain Portland cement after 28 days. In addition, a previous study [7] showed the reduction of chloride penetration of silica fume mortars and concretes in rapid chloride penetration tests (RCPTS). However, there are a few materials used in mine backfilling, and the research on these materials is limited.

The results showed that the stone powder is not completely inert diluent for the cement. A chemical reaction between $CaCO_3$, C_3A, and C_4AF generates $C_3A{\cdot}X{\cdot}CaCO_3{\cdot}11H_2O$ and ettringite [8]. As the center of hydration process, stone powder can increase the early rate and degree of hydration [9]. In addition, SPC results in a smaller consumption of water than that of the cement of the same standard; when comparing the bleeding rate of SPC and ordinary cement, Albeck and Sutej [10–12] found that the bleeding rate of SPC is always less than that of the ordinary cement, and it also stops bleeding more quickly. According to El-Didamony et al. [13], the set time of cement decreases with the increase in the stone powder content, which means that the SPC has a high early strength. Consequently, as substituted minerals are added in the cement paste, stone powder can promote the hydration of cement, induce the crystallization of cement hydrate products, accelerate the hydration of cement, and participate in the hydration reactions [14]. Previous studies have found that the powder of silicate minerals could be used as sustainable replacements of cement. Abd Elmoaty et al. [15] used granite dust to replace cement with 5–15%, which could improve concrete's compressive strength and tensile strength. Kannan et al. [16] reported that high-performance concrete can be produced with significant replacement of between 20% and 40% of Portland cement with ceramic waste powder. Berriel et al. and Akhlaghi et al. [17, 18] showed that a combination of calcined clay, limestone, and gypsum, used as the substitution of Portland cement for up to 50%, can provide economic benefits while maintaining the mechanical properties of the cement. However, if the stone powder content exceeds a certain value, the water demand of the cement paste will increase, and the fluidity will reduce. Therefore, in the current work, the possibility of reasonably using waste stone powder as a partial replacement for cement has been explored. The comprehensive use of stone powder having the same main ingredients as the mother rock conforms to the concept of green building materials and is conducive to sustainable developments in the construction industry [19, 20].

Based on the abovementioned properties of SPC, the experimental study of stone powder cement tailings backfill (SPCTB) can be developed. In this study, the physicochemical properties and the particle-size distribution of stone powder and tailings were analyzed using X-ray fluorescence (XRF) and laser particle size analyzer (LPSA). In addition, the strength characteristics of backfill with different ratios were analyzed to evaluate the feasibility of SPC used as the cementitious material. The microscopic morphology, composition, water evolution, and pore changes of SPCTB at different ages were examined, and the reaction mechanism of SPCTB was studied using X-ray diffraction spectroscopy (XRD), scanning electron microscopy (SEM), and nuclear magnetic resonance (NMR). The use of SPC as the cementitious material not only reduces the backfilling costs for mountainous mines but also benefits the construction of "green mines" and achieves no-waste mining.

2. Experimental

2.1. Tailings, Stone Powder, and Cement. Tailings were obtained from Gaofeng mine in Guangxi Province, China, and were divided into two types (tailings A and tailings B). The types of tailings were produced by different beneficiation processes. The stone powder was obtained from the

(a) (b) (c)

Figure 2: Physical appearance of (a) tailings A, (b) tailings B, and (c) stone powder.

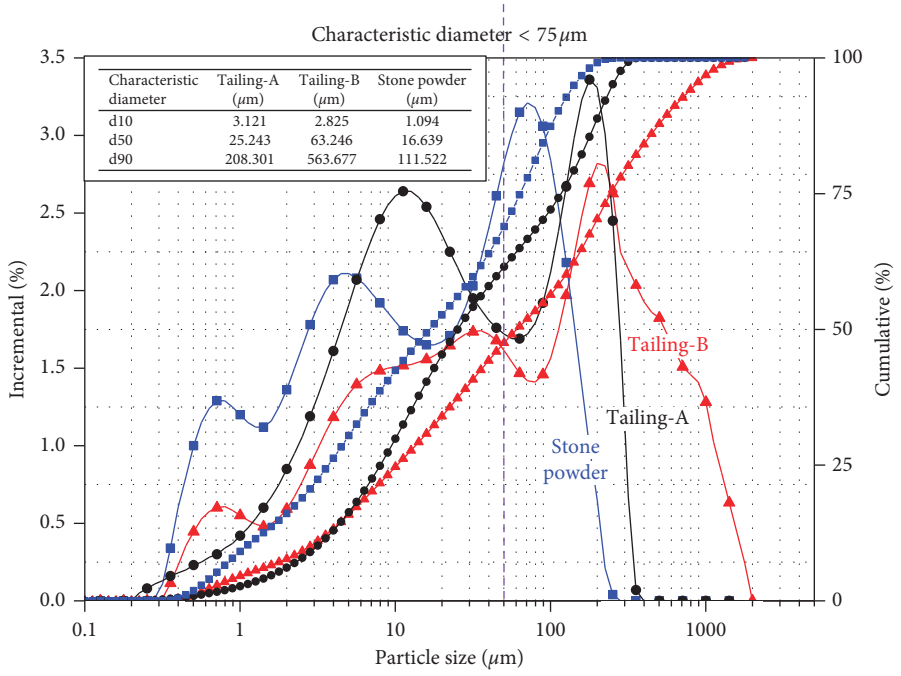

Figure 3: Particle-size distributions of tailings and stone powder (including incremental and cumulative values).

quarry around the Gaofeng mine (Figure 2). The particle-size distributions of the tailings and the stone powder were analyzed using a mastersizer 2000 obtained from Malvern Instruments Inc., UK (Figure 3). The characteristic median diameters d_{50} of tailings A and tailings B were 25.243 μm and 31.168 μm, respectively, based on which the tailings could be considered as ultrafine tailings. The median diameter d_{50} of the stone powder was 16.639 μm due to which it belonged to the category of ultrafine particles. The nonuniformity coefficient (Cu) and the curvature coefficient (Cc) of tailings A and tailings B were (14.56, 0.72) and (40.02, 0.71), respectively, indicating that the gradation of tailings A was good, though the tailings B had a wider range.

The apparent density, the bulk density, and the contents of surface water of tailings and stone powder were analyzed according to the standard *GB/T 50080-2016* "Standard Test Method for Performance of Ordinary Concrete Mixtures." The corresponding results are presented in Table 1. The elemental and chemical compositions of tailings and stone powder were obtained using XRF and XRD, and the respective results are provided in Table 2 and Figure 4. According to the chemical composition index [21], the alkaline coefficients of tailings A, tailings B, and stone powders were 3.21, 0.53, and 1.53, respectively. These results showed that tailings A belonged to the alkaline tailings and tailings B belonged to the acid tailings.

The cement from the Xinxing cement factory in Changsha, China, meets the national standard *GB 175-2007* "Common Portland Cement." The mineral composition of the cement is provided in Table 2. Furthermore, tap water was used for the experiments.

Table 1: Physical properties of the tailings and the stone powder.

Class	Apparent density	Packing density	Surface moisture content
Tailings A	3.49	1.24	0.128
Tailings B	2.77	1.17	0.135
Stone powder	2.89	0.99	0.162

Table 2: Elemental composition of the tailings and the stone powder along with the chemical composition of Portland cement (%).

Elemental composition	O	Fe	S	Ca	Si	Mg	Al
Tailings A	34.699	23.098	15.857	14.025	4.476	2.117	1.113
Tailings B	44.376	12.662	8.877	9.091	16.24	0.403	3.057
Stone powder	58.301	0.942	0.298	23.279	14.901	0.471	1.273
Chemical composition	$3CaO{\cdot}SiO_2$		$2CaO{\cdot}SiO_2$		$3CaO{\cdot}Al_2O_3$	$4CaO{\cdot}Al_2O_3{\cdot}Fe_2O_3$	
Portland cement	52.8		20.7		11.5	8.8	

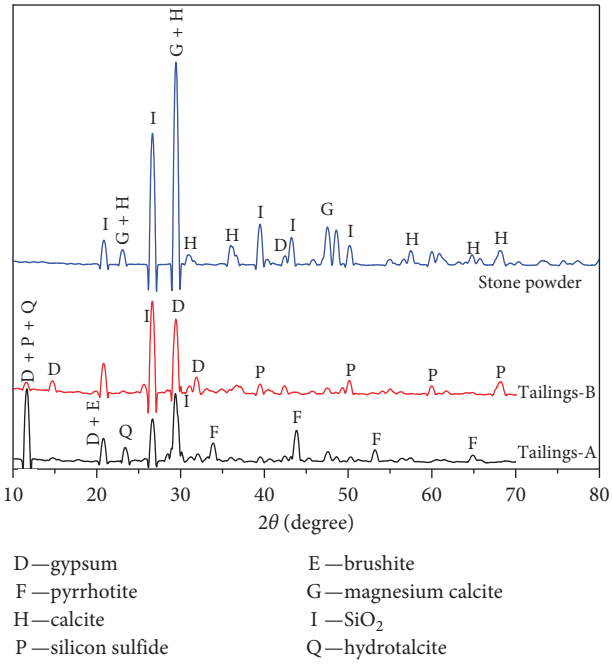

Figure 4: XRD patterns of the tailings and stone powder.

2.2. Specimen Preparation. In this work, SPC and the tailings were used as the cementitious material and the aggregate, respectively. The ratios between the two materials, which were tested in this work, are presented in Table 3. The SPC tailings ratio `(SPCTR), the mass fractions, and the stone powder dosage of Group A using tailings A and those of Group B using tailings B were the same.

The SPCTB components, including stone powder, cement, tailings, and water, were weighted using a high-precision electronic scale having an accuracy of 0.01 g. Mixtures with 10 different formulations (mixing ratios) were mixed in the laboratory blenders for 5 min to ensure homogeneity. Then, the mixtures were casted in plastic cubical molds with the side length of 7.07 cm. A total of 180 sextuplicate specimens (three for UCT and three for NMR) were prepared (Figure 5). The specimens were cured in a humidity chamber at 20°C and 95% relative humidity for different durations (3, 7, and 28 days) until the prescribed age reached. After that, the samples were analyzed for their physicochemical properties.

Table 3: Backfilling slurry of stone powder cement tailings ratio (SPCTR), mass fractions, stone powder content, and cement content.

Group	SPCTR	Mass fractions (%)	Stone powder content[a] (%)	Cement content (%)
A/B 1	1 : 4	70	0	100
A/B 2			10	90
A/B 3			15	85
A/B 4			20	80
A/B 5			100	0

[a]The proportion of stone powder in SPC.

2.3. Uniaxial Compressive Tests. The uniaxial compressive strength (UCS) at a given time is the most important parameter to evaluate the mechanical performance of SPC. Until the predetermined curing time, the SPCTB specimens were analyzed for USC using a computer-controlled universal pressure mechanical device (WDW-2000). The tests were performed following the procedure given in the standard *ASTM D2166/D2166M-16*. The specimens were loaded under a constant vertical displacement rate of 1 mm/min. To reduce the error, the tests were conducted in triplicates, and the average values were used to determine the UCS of SPCTB (accurate to 0.1 MPa) (Figure 6). The individual strengths of three specimens, molded with the same characteristics, should not deviate more than 15% from the mean strength.

2.4. NMR Analysis. During the hardening of backfilling slurry, the water, pore distribution, and strength of the backfilling slurry would change with age, and backfill is formed after hardening. The UCS of the backfill is closely related to the water content in different binding states. The NMR, performed using 1 H relaxation signal, can be used to

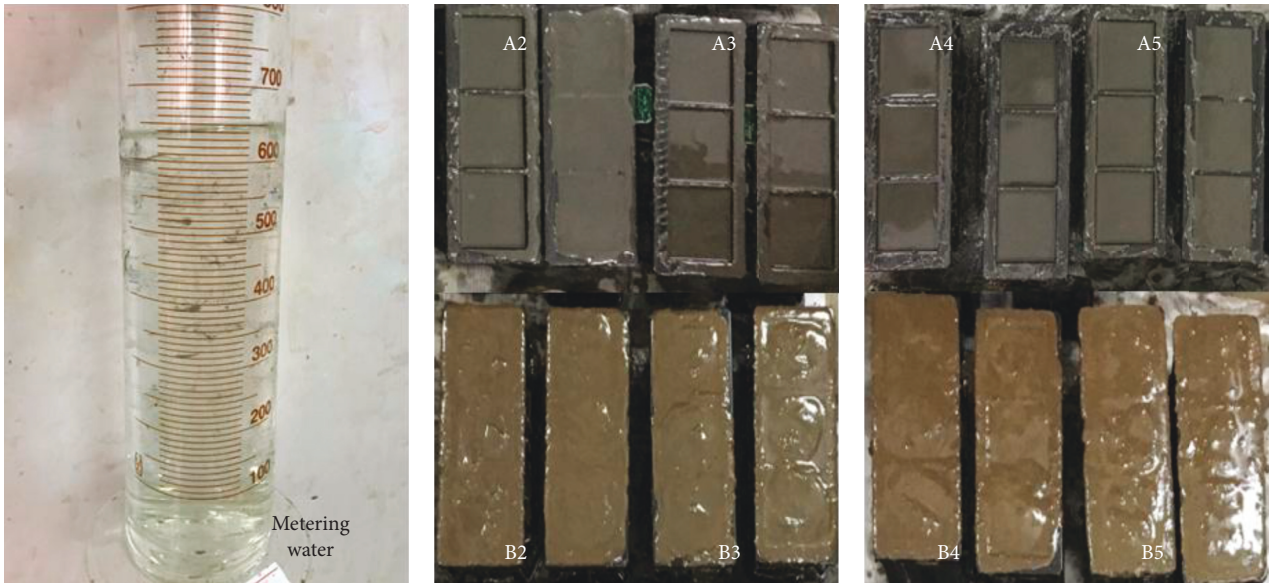

(a) (b) (c)

Figure 5: Production process for the backfill (including metering water and backfilling paste).

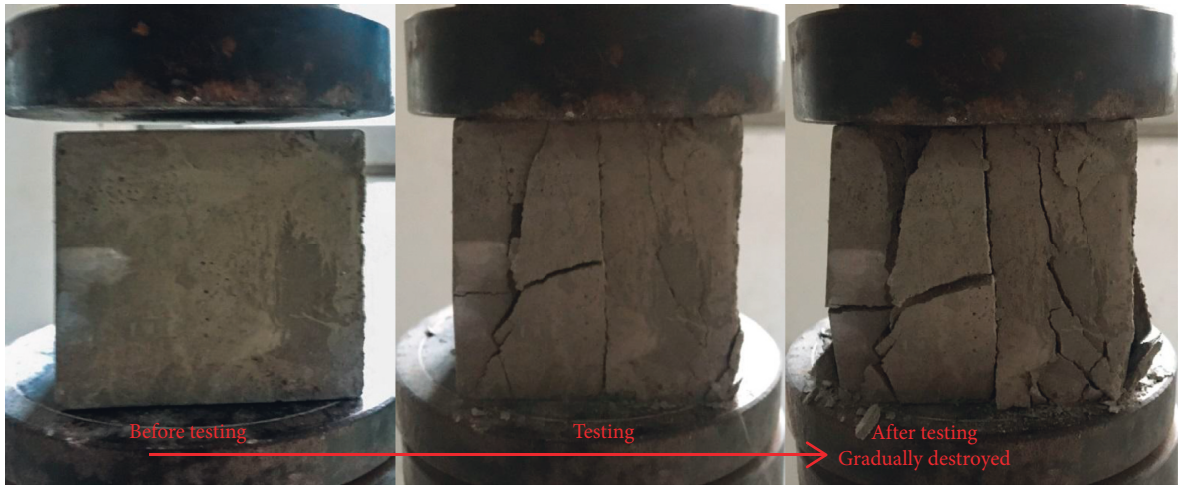

Figure 6: UCT and destruction process of a 28-day SPCTB specimen containing 10% stone powder.

measure the porous content in the slurry and the backfill. The T2 distribution can be used to analyze the variation in pore distribution, which has the advantages of non-destructive detection and good repeatability [22].

The NMR tests used the MiniMR-60 magnetic resonance imaging (MRI) analysis system, which was manufactured by Shanghai Newmai Co. Ltd., China. The main magnetic field of the device was 0.51 T, and the H proton resonance frequency was 21.7 MHz.

The analysis was performed in triplicates, and the average value for further analysis was calculated. After the SPCTB specimens reached the specified age (3 d, 7 d and 28 d), the SPCTB specimens were taken out from the constant temperature and constant humidity curing box and subjected to NMR relaxation measurements. During the tests, the SPCTB specimens were wrapped in a cling film to reduce the impact of water evaporation.

2.5. SEM and XRD Analyses. At the curing times of 3 d, 7 d, and 28 d, the SPCTB specimen of 1 mm^2 area was taken from the core of the specimen and dehydrated with absolute ethanol to stop the hydration. The specimen was dried at 45°C to constant weight and analyzed using XRD and SEM analyses. The experiments used a Siemens D500 X-ray diffractometer and a TESCAN MIRA3 field-emission scanning electron microscope for these analyses.

3. Strength Characteristics

The (statistical) average strength of each group of specimens and part of the stress-strain curves of these specimens are shown in Figures 7 and 8, respectively.

(1) At the curing time of 3 days (d), the UCS of Group A was 0.4-0.5 MPa, while that of the Group B was

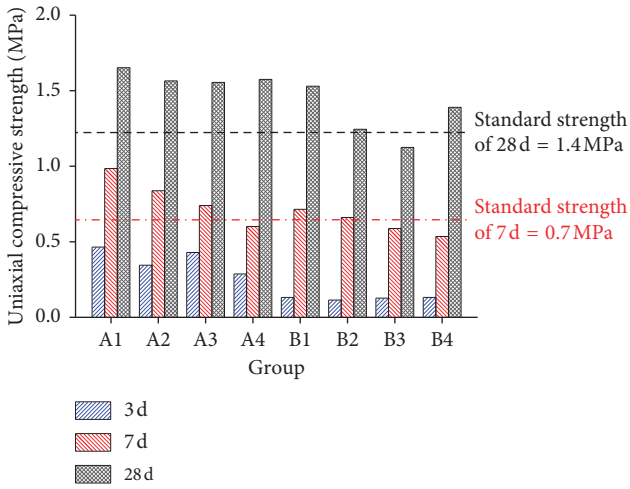

Figure 7: Uniaxial compressive strength of each group of specimens at the curing times of 3 d, 7 d, and 28 d (according to the mine information 7 d and 28 d compressive strengths need to reach 0.7 MPa and 1.4 MPa, respectively. A5 and B5 groups are not analyzed for compressive strength).

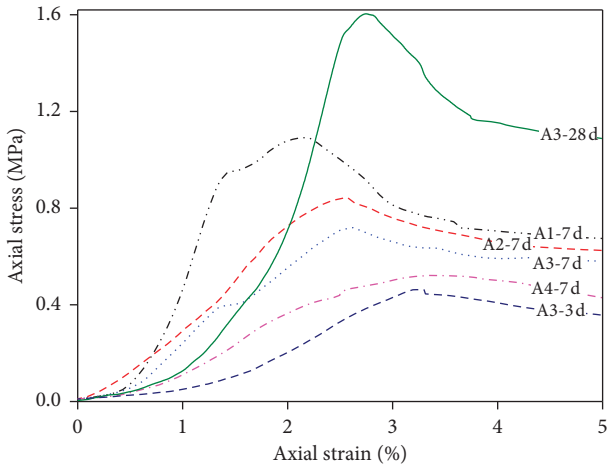

Figure 8: Stress-strain curves at the curing time of 7 d of Group A and at the curing times of 3 d and 28 d of Group A3.

0.2 MPa. At the curing time of 7 d, the USC of Group A was 0.6–1.0 MPa, whereas that of Group B was 0.6–0.7 MPa, which gradually decreased with the increase in the content of stone powder. At the curing time of 28 d, the UCS of Group A was 1.6–1.7 MPa, while the USC of SPCTB specimens mixed with the stone powder was basically the same as 1.6 MPa. The USC of Group B was 1.2–1.6 MPa, which tended to decrease with the increase in stone powder's USC. In addition, the USC suddenly increased to 1.5 MPa at the stone powder content of 20%.

(2) The minimum requirements for the backfill strength of mine stopes at the curing times of 3 d, 7 d, and 28 d were 0.25 MPa, 0.7 MPa, and 1.4 MPa, respectively. Group A met the 3 d backfill strength requirements, while the strength's value for Group B was too low. The content of stone powder in Group A was varied to values of 0%, 10%, and 15%, while Group B1, which was not doped with stone powder, satisfied the requirements of 7 d backfill strength. While for the curing time of 28 d, only Groups B3 and B4 did not meet the backfill strength requirements. Furthermore, Groups A1, A2, and A3 met the requirements of the backfill strength with less than 15% of the stone powder content. The backfill strength of groups that met the requirements had a certain safety factor, which could be changed according to the actual conditions of the stopes and was based on the minimum requirements of the mine. The ratio of the backfill material and the content of the stone powder were adaptable to the environmental parameters of the stopes, which ensured that safe and efficient recovery of backfill material ratio parameters can be selected for the mine.

(3) The intensity ratio after the curing times of 3 d, 7 d, and 28 d for Group A gradually changed from 1 : 2 : 4 to 1 : 2 : 6 with the increase in the content of stone powder. After the stone powder was mixed, the UCS of the SPCTB specimens was reduced, which increased rapidly after 7 days. Additionally, the more the powder added, the faster the increase in the USC value.

(4) With the increase in the content of stone powder, the peak strength and the elastic modulus of the specimen gradually decreased. In addition, the peak strength appeared under the condition of larger strain. The strength and the elastic modulus of the specimens after the curing time of 3 d were low, and the plastic deformation of the specimens was large. The elastic modulus of Group A3 after the curing time of 28 d was lower than that of Group A1 after 7 d. The increase in the content of stone powder reduced the elastic modulus of the backfill. The residual strengths of the six groups of backfill specimens in the postfailure were large and decreased slowly and gradually to stable values, which ensured that the backfill had sufficient strength to keep the backfill and stopes stable.

4. Results and Discussion

4.1. Various States of Bound Water. With the hydration of backfilling slurry, a part of the water in the slurry did not participate in the hydration reaction, which was either secreted or evaporated into the air. The rest remained in the backfill. Water in the hydration backfilling slurry was divided into free water, capillary water, adsorbed water (physical adsorption through hydrogen bonding), interlayer water, and chemically bound water. The loss of water gradually increased as the fluidity of the water gradually deteriorated.

After the NMR sampling, the T2 distribution of the slurry, which was obtained by T2 inversion software, is shown in Figures 9(a) and 10(a). In these figures, the horizontal axis is the relaxation time T2, while the vertical axis is the signal intensity. The peaks from left to right are defined as Peak 1, Peak 2, and Peak 3. Previous relevant studies have shown that different bound states have different T2

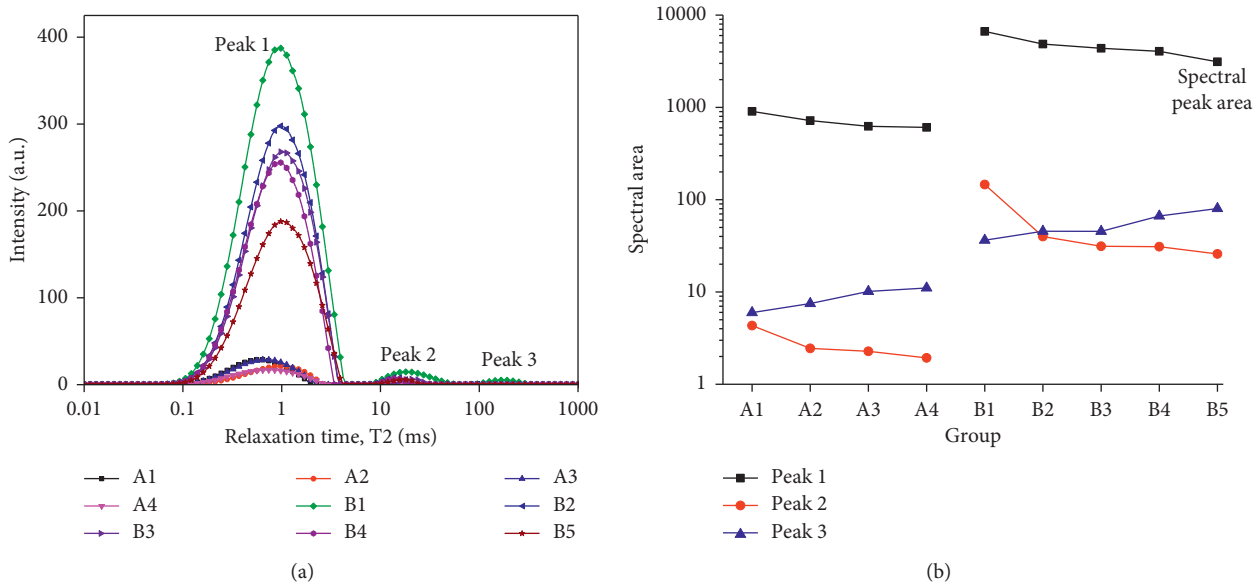

Figure 9: (a) NMR T2 spectrum distribution and (b) areas of Peak 1, Peak 2, and Peak 3 after the curing time of 3 d.

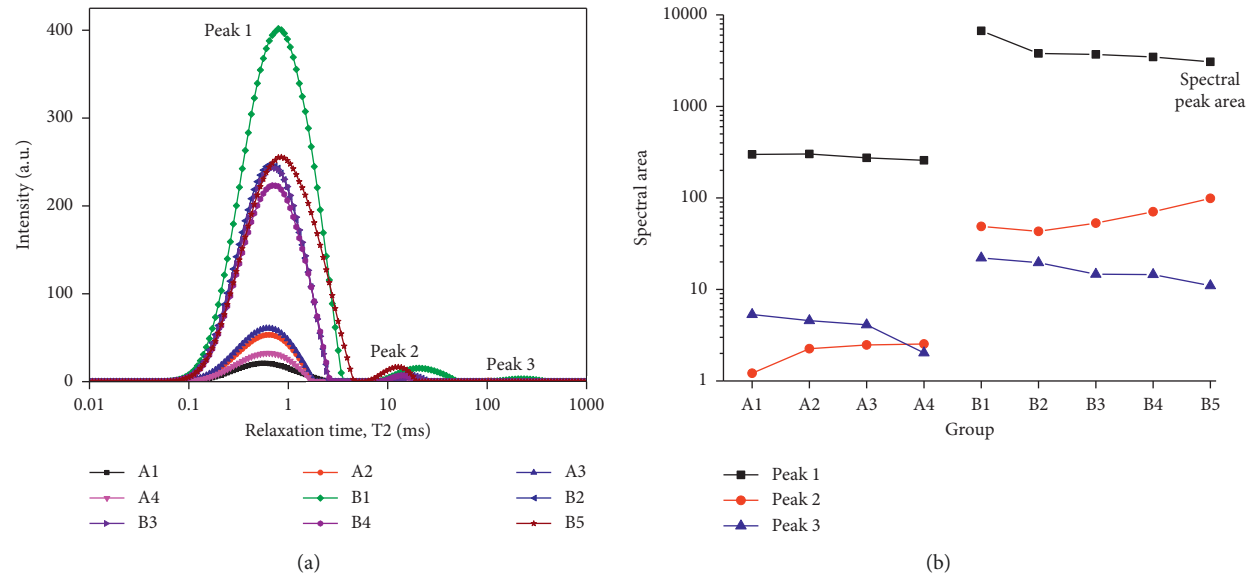

Figure 10: (a) NMR T2 spectrum distribution and (b) areas of Peak 1, Peak 2, and Peak 3 after the curing time of 7 d.

distributions of water. Each peak represents a particular bound state of water. The tighter the water bound is, the worse mobility the water has and the shorter the relaxation time T2 is [23–25]. Since the time of relaxation of chemisorbed water in the slurry and interlaminar water is short and the Carr–Purcell–Meiboom–Gill (CPMG) experiment cannot acquire the NMR signal, Peak 1 could be considered as the relaxation signal generated by the adsorbed water. Peak 2 was generated by the capillary water, and Peak 3 was generated by the free water. The relaxation time represented the various states of bound water, whereas the signal intensity represented the content of water and the spectral area represented the content of water of the same type.

(1) The relaxation times of Peak 1 of Groups A and B were nearly the same, followed by those of Peak 2 and Peak 3. In the T2 spectrum, the amplitudes, the signal peak intensities, and the peak areas of Peak 1 and Peak 2 in Group B were larger than those in Group A, which indicated that there were more adsorbed water and capillary water in Group B. With the increase in the curing time, the relaxation time did not change significantly, and the peak amplitude decreased, indicating that the contents of various types of water in the backfill specimen decreased with the increase in curing time. In Groups A and B, the proportion of Peak 1 was more than 97%,

indicating that the majority of adsorbed water was contained in the backfill specimen.

(2) After the curing time of 3 d, the contents of adsorbed water and capillary water in the backfill specimen gradually decreased with the increase in the content of stone powder, while the content of free water increased. Under the same proportioning parameters, the content of bound water in Group B exceeded than that in Group A, which indicated that different tailings had some influence on the change in water content in the backfill specimen.

(3) Since some free water adsorbed on the stone powder particles (SPPs) after 3 d, which caused the decrease in capillary water and the content of adsorbed water in the system, there was no medium for hydration reaction and the rate of hydration reaction was reduced. The adsorbed water and the free water in the backfill specimen decreased with the increase in the content of stone powder, whereas the content of capillary water increased as well. However, with the hydration reaction going on, the free water adsorbed on SPP gradually entered the pores and became the medium of hydration reaction. This was also the reason why the strength of SPCTB increased significantly in the later stage of the addition of stone powder.

The three peak relaxation time ranges and the corresponding water categories are provided in Table 4. Each group NMR T2 spectrum distribution and the peak areas after the curing times of 3 d and 7 d are shown in Figures 9 and 10.

4.2. Analysis of the Pore Structure. The microstructure of the cross section of the specimen with different proportions after 28 d was obtained using SEM with the magnification of 5000 times. Figures 11(a) and 11(b) show the two micromorphologies of Groups A4 and B4. The results show that the gelled structure was fairly compact, though there were some pores around the particles. As can be seen, the structural stability was good when the particles were densely packed. The cementing mesh structure was compact, and the pores were small. The gray areas in SEM images were small, based on which the variation in plane porosity in different proportions can be observed [26, 27].

The images were binarized to ensure the preciseness of the pore results. The process is also known as the threshold segmentation. In view of the differences between the grayscale distribution and the values of the pixels of the particles, the cementing structure, and the pores, the pores in the image could be calculated using the binarized image. Assuming that the size of the SEM image was $M \times N$, $f(x)$ represented the gray area of the pixel located in the line $(x-1)$ and column $(y-1)$ of the image. The principle of binarization of the SEM image is given as follows:

$$f(x,y) = \begin{cases} 0, & f(x,y) < T, \\ 1, & f(x,y) > T, \end{cases} \quad (1)$$

where T represents the threshold grayscale. The SEM image can be binarized and converted to a black-and-white image, which is represented by a matrix of black-and-white pixels, in which 0 is the white pixel and 1 is the black pixel, and represents the pores and particles, respectively. With the help of Image-Pro Plus software, and for the threshold of 35, the SEM image of every group was processed (Figures 11(c) and 11(d)). The number and the area of pores contained within each group were calculated, and the plane porosity was determined. Each image consisted of four sets of data in four different positions to avoid any accidental error. The plane porosities of Groups A and B were linearly fitted and are shown in Figure 12.

Table 4: Relaxation time range of Peak 1, Peak 2, and Peak 3 and the corresponding bound state water.

Peak	Peak 1	Peak 2	Peak 3
Relaxation time range, T2 (ms)	0.3~3	7~60	78~310
Bound-state water	Adsorbed water	Capillary water	Free water

(1) Fitting curves of Groups A and B are represented by the equations: $Y = 0.1594X + 2.033$ and $Y = 0.8894X + 8.178$, respectively. It can be seen that the plane porosities of Groups A and B gradually increased with the increase in the content of stone powder, which led to the decrease in the intensity of the SPCTB specimen.

(2) For the same ratio, the plane porosity of Group B was larger than that of the Group A. Because of this, not only the stone powder but also the nature of tailings will have an effect on the change in pores. The plane porosity of Group B increased faster, indicating that the addition of stone powder exhibited a greater influence on the plane porosity of SPCTB made up of tailings B.

4.3. Analysis of the Hydration Products. The results for the component analysis (done using XRD) are shown in Figure 13. The figure shows the hydration products of backfill specimens after different curing times. Based upon the results, the following conclusions can be drawn:

(1) There was no hydration product in the backfill in the absence of cement, indicating that the stone powder was in an inert state, and therefore, the hydration reaction did not occur. Gypsum existed throughout the hydration process, while in CTB and SPCTB, gypsum almost disappeared after the curing time of 28 d, indicating that the gypsum in tailings and the cement were involved in the hydration reaction.

(2) Some C-S-H gel dispersions and hydroxide diffraction peaks appeared in the SPCTB and CTB after the curing time of 3 d, though they were not very obvious. With the increase in the hydration time, some dispersive peaks with low intensity and discrete diffraction angles appeared after the curing time of 28 days. These were ascribed to C-S-H dispersion. At the same time, there was an increase in the diffraction

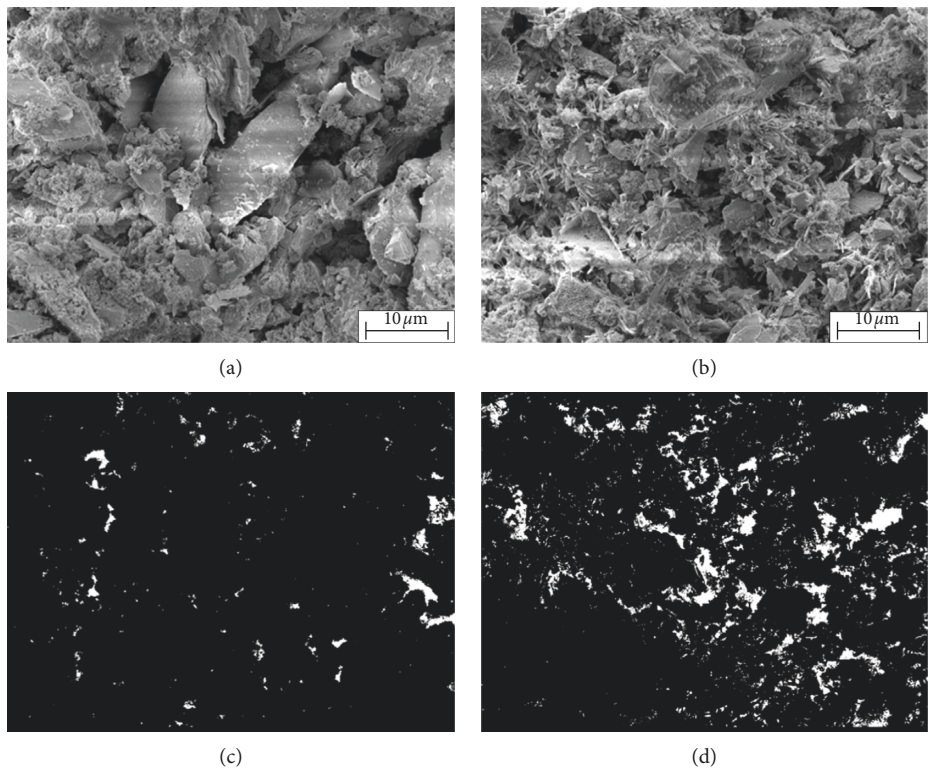

Figure 11: Microtopography and its binarized image; (a) magnified SEM image of Group A4; (b) magnified SEM image of Group B4; (c) Group A4 after binarization; (d) Group B4 after binarization.

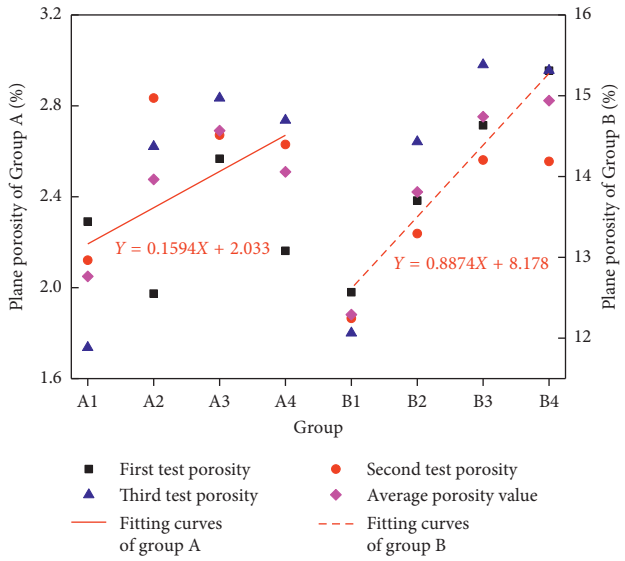

Figure 12: Plane porosity of each group and the fitting curves of the plane porosity of Groups A and B after the curing time of 28 d.

peak of the hydroxide, which indicated that the hydration reaction continued with the increase in curing time. AFt and some AFm in hydration products after the curing time of 3 d gradually decreased after 7 d and 28 d, which indicated that the hydration products at the early stage were mainly AFt, while at the later stage, they were the C-S-H gel.

(3) Comparing Figure 13(a) with Figure 13(b), it can be seen that the intensities of AFt and AFm diffraction peaks in SPCTB were weaker at 3 d, while AFt was the main reason for the early strength of backfill. Therefore, the early strength of SPCTB would be lower. At 28 d, $Ca(OH)_2$ diffraction peaks were weaker and C-S-H gel dispersion peaks were basically the same, indicating that the stone powder consumed $Ca(OH)_2$ to generate C-S-H gel after the hydration reaction, which was more stable than AFt. This ensured the poststrength and volume stability of SPCTB.

4.4. Analysis of the Micromorphology. Figure 14 shows the microstructural and micromorphology features of different cementitious materials at different curing times. Based upon the results, the following conclusions are drawn.

(1) For the curing time of 7 d, a large amount of hydration products, including a large amount of acicular AFt crystals, some amorphous C-S-H gel, some stone powder, and tailings particles were formed in the CTB and SPCTB. Acicular AFt crystals grew on the surface and in the pores of the particles, which developed into a three-dimensional (3D) network structure that was covered with SPP and tailings particles, having some early strength. AFt of the SPCTB acicular crystal grew sparser, though the microstructure was more compact than the CTB. This was due to the reason that the

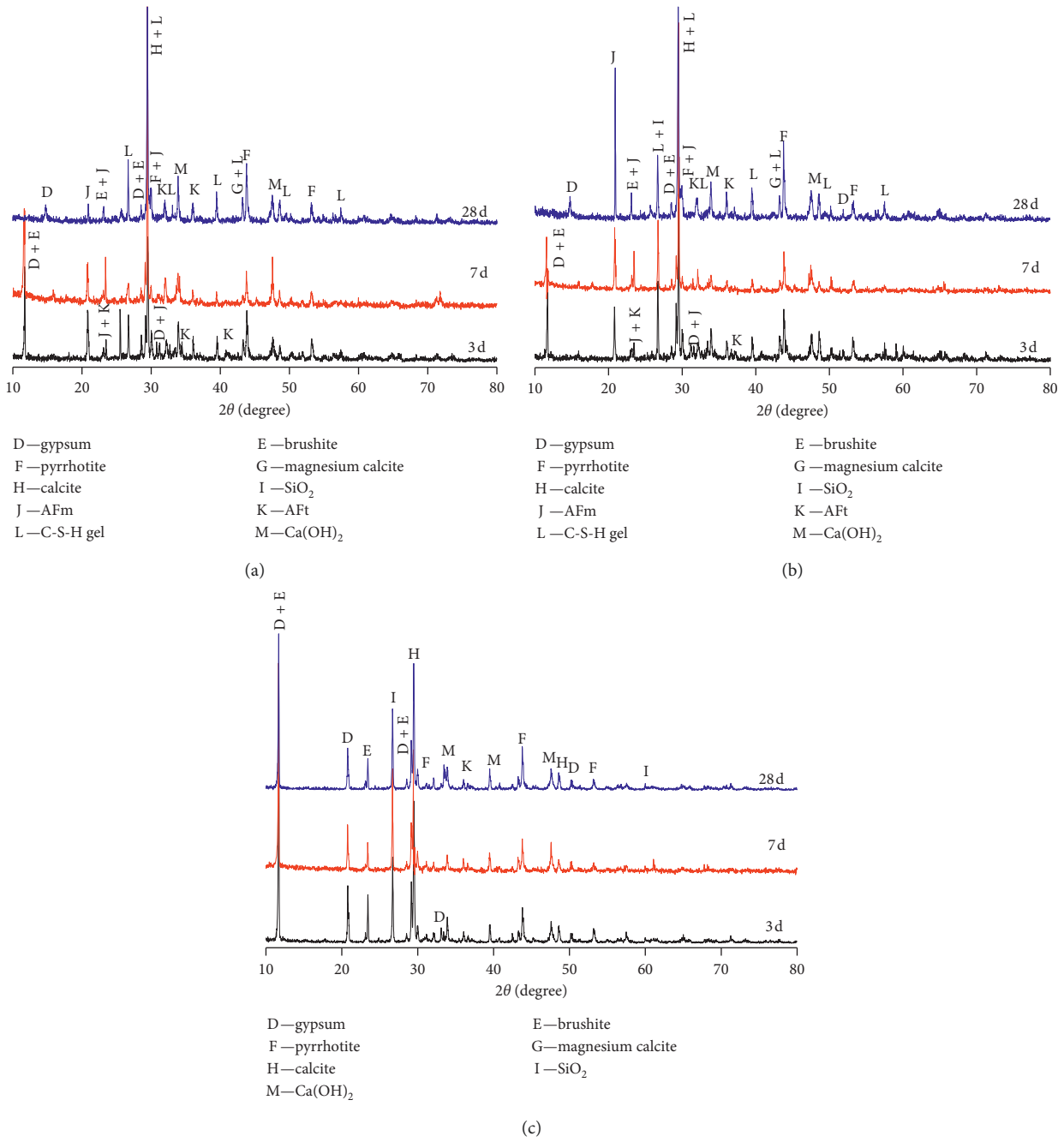

Figure 13: XRD patterns of the hydration products; (a) cement tailings backfill (CTB); (b) stone powder cement tailings backfill (SPTB). AFt represents ettringite; AFm represents monosulfate hydrate.

shape of SPP can fill the pores formed by the rod-shaped tailings particles.

(2) For the curing time of 28 d, the AFt crystals of acicular structure almost disappeared. The amorphous C-S-H gel grew on the surface of tailing particles and closely combined with it. Compared with the results for the curing time of 7 d, the microstructure was more compact. The strength of backfill and the other aspects were improved for amorphous and rod-like C-S-H gel structure, which grew in the original pores and was tightly combined with the tailings particles. The SPP became obscure, while the smooth surface became uneven, indicating that the stone powder reacted with the hydration products to generate secondary products. The growth of a rod-like structure in the pores and the overall absence of obvious pores indicated that the microstructure was basically similar to that of the CTB.

4.5. Reaction Mechanism of SPC in Backfill. According to the different times and the characteristics of hydration between the SPCTB and CTB, the hydration process of backfilling material system can be divided into following four stages:

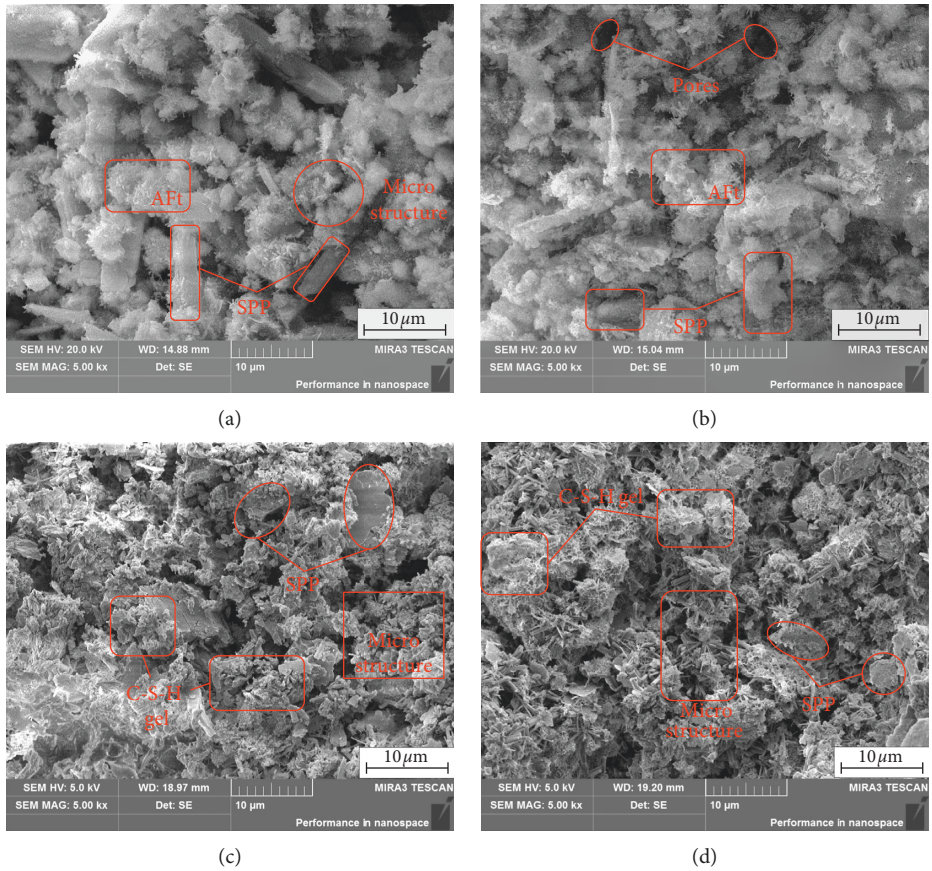

Figure 14: SEM image of the hydration product in the backfill; (a) CTB at 7 d; (b) SPCTB at 7 d; (c) CTB at 28 d; (d) SPCTB at 28 d.

dissolution period, condensation period, infiltration period, and hardening period. Figure 15 shows the model of hydration process of SPCTB.

(1) *Dissolution Period.* One mechanism [28] of hydration of Portland cement shows that the through-solution hydration involves the dissolution of anhydrous compounds into their ionic constituents, which results in the formation of hydrates in the solution. This phenomenon happens due to their low solubility and eventual precipitation of the hydrates from the supersaturated solution. From SEM images of 3D hydrating cement pastes (Figure 15), it appears that the through-solution mechanism is dominant in the early stages of cement hydration. The hydration reactions are most violent during the dissolution period. C_3A and C_4AF in the cement particles dissolved first and produced large amounts of $[AlO_4]^-$, $[SO_4]^{2-}$, $[Ca]^{2+}$, and $[OH]^-$ ions. However, both SPP and tailings dissolved in water containing these ions. Water acted as a reaction medium in the violent hydration reaction of these ions.

(2) *Condensation Period.* Depending on the concentration of aluminate and sulfate ions in the solution, the precipitating crystalline product is either calcium aluminate trisulfate hydrate or calcium aluminate monosulfate hydrate. In solutions saturated with calcium and hydroxyl ions, the former crystallizes as short prismatic needles and is also referred to as high sulfate or by its mineralogical name, ettringite (AFt crystals). The monosulfate is also called low sulfate and crystallizes (AFm crystals) as thin hexagonal plates. The relevant chemical reactions may be expressed using the reaction equations [28].

Ettringite:

$$[AlO_4]^- + 3[SO_4]^{2-} + 6[Ca]^{2+} + \text{aq.} \longrightarrow C_6A\overline{S}_3H_{32} \quad (2)$$

Monosulfate:

$$[AlO_4]^- + [SO_4]^{2-} + 4[Ca]^{2+} + \text{aq.} \longrightarrow C_4A\overline{S}H_{18} \quad (3)$$

The hydration reaction produced a large number of acicular AFt crystals and hexagonal plate-shaped AFm crystals. AFt is the main cause of the early strength of the specimens and represents the generation of AF. It is also the beginning of coagulation period and reaches the final coagulation state until the complete formation of AFt crystals. At the same time, the hydration reaction will also generate a part of amorphous C-S-H gel, which is attached to the surface of tailings particles and SPP.

(3) *Infiltration Period.* At later ages of hydration reaction, when the ionic mobility in the solution becomes restricted, the hydration of residual

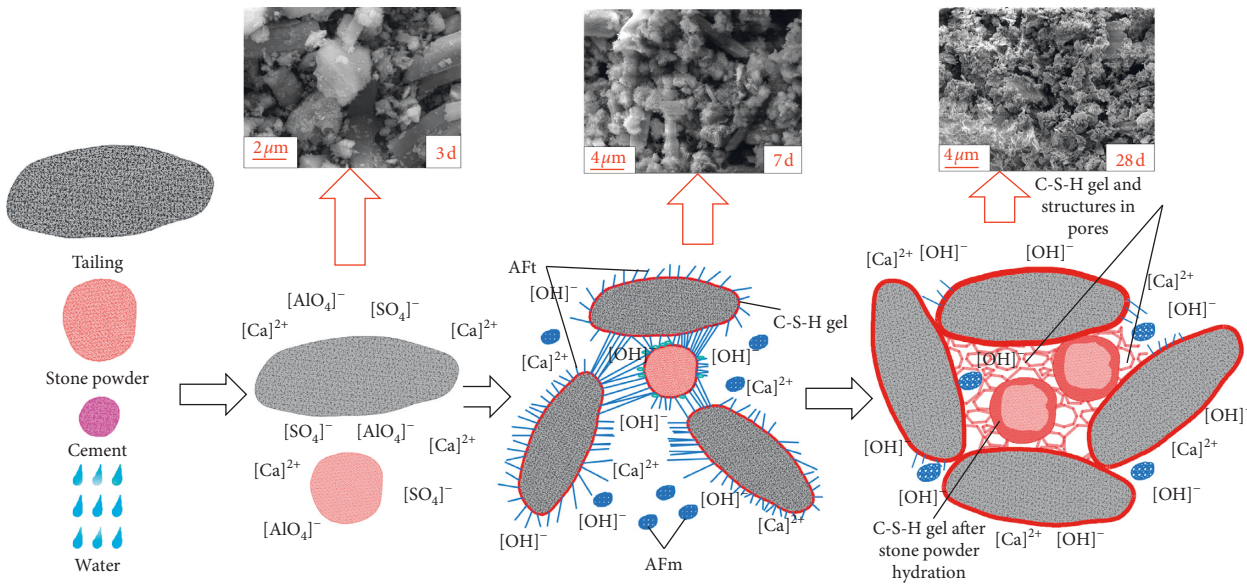

Figure 15: Model for the SPCTB hydration process.

cement particle may occur through solid-state reactions. Meanwhile, stone powder acts as nucleation sites for hydration products [29]. It is not surprising that the inclusion of stone powder increases the rate of hydration. At the same time, according to Section 4.3 of hydration products, the proportion of SiO_2 decreased in 7 d and 28 d, which means that SiO_2 reacted with hydration products. In this period, C_3S and C_2S in cement dissolve in water in large quantities and start the hydration reaction. A large amount of C-S-H gel, $[Ca]^{2+}$, and $[OH]^-$ are formed to produce the strong alkaline environment. AFt crystals and AFm crystals formed in the coagulation period under the strong alkaline environment rapidly dissolve and are converted into more stable C-S-H gel. The unstable structure of the surface of stone powder will be destroyed by the strong alkaline environment, and the strong alkali and active SiO_2 of stone powder react to generate C-S-H gel covering the surface of the stone powder. When the osmotic pressure and other factors are not sufficient to drive the continued inward layer reaction, the hydration reaction on the surface of the stone powder would stop. Figure 16 shows the relative amount of hydration products during hydration age.

(4) *Hardening Period.* According to the micromorphology analysis of 28 d, the products of C-S-H gel in the pores and on the surface of the stone powder are gradually formed, whereas the C-S-H gel of every part gradually contacts with other parts to form a stable 3D network-like gel structure, which tends to be stable. In this case, the reaction medium is the little amounts of capillary water and free water. Afterwards, the hydration reaction slows down, and the hydration reaction time continues to increase even for several years.

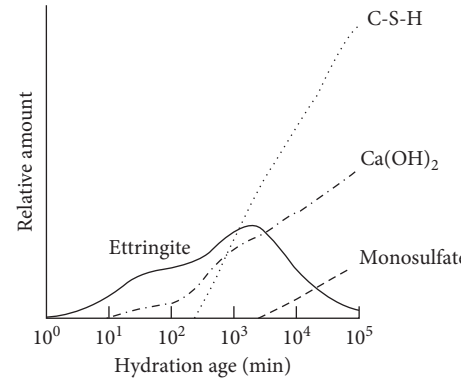

Figure 16: Relative amount of different hydration products during hydration age.

During the condensation period, the amount of the cement SPP system is relatively small, and many parts are needed to be cemented. The existing infiltration period slows down the rate of hydration reaction, resulting in low early strength of the SPC system. In the later stage of the infiltration period and the hardening period, the stone powder begins to participate in the hydration reaction, and the strength of the SPC system increases rapidly. At present, the strength has been analyzed only for the curing time of 28 d, while the increasing trend of strength even after 28 d has not been studied. This part of the experiment needs to be studied in a future work to further discuss the reaction mechanism of the SPC in backfill.

5. Conclusions

In this paper, the backfill specimens consisting of stone powder, cement, and tailings were analyzed to study whether the strength of SPCTB meets the requirements of mine backfilling or not. The reaction mechanism of SPC in

backfilling slurry hardening process has also been analyzed. The analysis was conducted using techniques, including uniaxial compressive tests (UCTs), nuclear magnetic resonance (NMR), scanning electron microscopy (SEM), and X-ray diffraction (XRD). The main conclusions are as follows:

(1) With the increase in the stone powder content, the strength of each age gradually decreases, whereas different types of tailings also affect the strength of backfill specimens. The strength of Group A with the content of stone powder less than 15% meets the requirements of mine backfilling strength, and therefore, it is more practical for potential applications in mines. The incorporation of stone powder will reduce the early strength of the backfill specimens, while it promotes the strength growth during the hydration reaction in the middle and later stages.

(2) The incorporation of the stone powder will affect the proportion of all kinds of bound states of water in the backfill specimens. With the increase in the stone powder content, the adsorbed water decreases gradually, while the capillary water increases at 3 d, which reduces the rate of hydration reaction. However, it decreases for 7 d period, which results from the free water adsorbed on SPP that gradually enters the pores and becomes the medium of hydration reaction. This was also the reason why the strength of SPCTB increased significantly in the later stage of the addition of stone powder.

(3) The incorporation of stone powder will increase the plane porosity of backfill specimens for 28 d curing period, which will lead to the decrease of strength. Different types of tailings will affect the plane porosity. The backfill specimens consisting of tailings B have larger plane porosity.

(4) When only the stone powder is used as the cementitious material, the hydration reaction would not occur, while the hydration reaction occurred in Groups 2, 3, and 4. The results showed that SiO_2 contained in stone powder reacted with hydration products at later stages of hydration reaction. The hydration products of SPCTB were mainly AFt at the early stages and amorphous C-S-H gel in the final stage. The stone powder particles disappeared in the final stage, indicating that the stone powder reacted with the cement hydration product in the middle and later stages. Additionally, it participates in the hydration reaction, which further promoted the increase in strength of the backfill specimens. Meanwhile, the C-S-H gel and the stone powder hydration products are closely combined, forming a close three-dimensional mesh structure.

(5) The hydration process of the backfilling material system can be divided into following four stages: dissolution period, condensation period, infiltration period, and hardening period. At the third and fourth stages of hydration reaction, the stone powder acts as nucleation sites for the hydration products. At the same time, the unstable structure of the surface of stone powder will be destroyed by the strong alkaline environment, and the strong alkali and active SiO_2 of stone powder react to generate C-S-H gel covering the surface of the stone powder. When the osmotic pressure and other factors are not sufficient to drive the continued inward layer reaction, the hydration reaction on the surface of the stone powder would stop.

Data Availability

The data used to support the findings of this study are available from the corresponding author upon request.

Conflicts of Interest

The authors declare that there are no conflicts of interest regarding the publication of this paper.

Acknowledgments

This research was supported by the National Key Research and Development Program of China (2017YFC0602901), National Key Technology Support Program (2015BAB12B01), and National Natural Science Fund (41672298) funded by Ministry of Science and Technology of the People's Republic of China and the Postgraduate Research and Innovation Foundation (2018zzts769) funded by Central South University.

References

[1] S. J. Choi, S. S. Jun, J. E. Oh, and P. J. M. Monteiro, "Properties of alkali-activated systems with stone powder sludge," *Journal of Material Cycles and Waste Management*, vol. 12, no. 4, pp. 275–282, 2010.

[2] G. Marchetti, V. F. Rahhal, and E. F. Irassar, "Influence of packing density and water film thickness on early-age properties of cement pasteswith limestone filler and metakaolin," *Materials and Structures*, vol. 50, no. 2, p. 111, 2017.

[3] M. J. Al-Kheetan, M. M. Rahman, and D. A. Chamberlain, "A novel approach of introducing crystalline protection material and curing agent in fresh concrete for enhancing hydrophobicity," *Construction and Building Materials*, vol. 160, pp. 644–652, 2018.

[4] M. J. Al-Kheetan, M. M. Rahman, and D. A. Chamberlain, "Development of hydrophobic concrete by adding dual-crystalline admixture at mixing stage," *Structural Concrete*, vol. 19, no. 5, pp. 1504–1511, 2018.

[5] A. A. Ramezanianpour, S. S. Mirvalad, E. Aramun, and M. Peidayesh, "Effect of four Iranian natural pozzolans on concrete durability against chloride penetration and sulfate attack," in *Proceedings of Second International Conference on Sustainable Construction Materials and Technologies*, Ancona, Italy, June 2010.

[6] A. Kumar and D. M. Roy, "A study of silica fume modified cements of varied fineness," *Journal of the American Ceramic Society*, vol. 67, no. 1, pp. 61–64, 1984.

[7] A. A. Ramezanianpour, A. Pilvar, M. Mandikhani, and F. Moodi, "Practical evaluation of relationship between

concrete resistivity, water penetration, rapid chloride penetration and compressive strength," *Constrution and Building Materials*, vol. 25, no. 5, pp. 2472–2479, 2011.

[8] S. Tsivilis, E. Chaniotakis, E. Badogiannis, G. Pahoulas, and A. Ilias, "A study on the parameters affecting the properties of Portland limestone cements," *Cement and Concrete Composites*, vol. 21, no. 2, pp. 107–116, 1999.

[9] I. Soroka and N. Stern, "Effect of calcareous fillers on sulfate resistance of Portland cement," *American Ceramic Society Bulletin*, vol. 55, no. 6, pp. 594-595, 1976.

[10] I. Mohammadi and W. South, "The influence of the higher limestone content of General Purpose cement according to high-strength concrete test results and construction field data," *Materials & Structures*, vol. 49, no. 11, pp. 4621–4636, 2016.

[11] H. El-Didamony, T. Salem, N. Gabr, and T. Mohamed, "Limestone as a retarder and filler in limestone blended cement," *Ceramics-Silikáty*, vol. 39, no. 1, pp. 15–19, 1995.

[12] J. Albeck and B. Sutej, "Characteristics of concrete made of portland limestone," *Beton- und Stahlbetonbau*, vol. 41, no. 5, pp. 240–244, 1991.

[13] H. El-Didamony, A. M. Sharara, E. Ebied, and A. El-Aleem, "Hydration characteristics of β-C_2S in the presence of some pozzolanic materials," *Cement and Concrete Research*, vol. 26, no. 8, pp. 1179–1187, 1996.

[14] C. Kemal, S. Hocine, E. H. Y. Yang, and V. C. Li, "Use of high volumes of fly ash to improve ECC mechanical properties and material greenness," *ACI Materials Journal*, vol. 104, no. 6, pp. 620–628, 2007.

[15] A. E. M. Abd Elmoaty, "Mechanical properties and corrosion resistance of concrete modified with granite dust," *Construction and Building Materials*, vol. 47, pp. 743–752, 2013.

[16] D. M. Kannan, S. H. Aboubakr, A. S. El-Dieb, and M. M. Reda-Taha, "High performance concrete incorporating ceramic waste powder as large partial replacement of Portland cement," *Construction and Building Materials*, vol. 14, pp. 435–441, 2017.

[17] S. S. Berriel, A. Favier, E. R. Domínguez et al., "Assessing the environmental and economic potential of limestone calcined clay cement in Cuba," *Journal of Cleaner Production*, vol. 124, pp. 361–369, 2016.

[18] O. Akhlaghi, T. Aytas, B. Tatli et al., "Modified poly(carboxylate ether)-based superplasticizer for enhanced flowability of calcined clay-limestone-gypsum blended Portland cement," *Cement and Concrete Research*, vol. 101, pp. 114–122, 2017.

[19] W. G. Shen, Y. Liu, L. H. Cao et al., "Mixing design and microstructure of ultra high strength concrete with manufactured sand," *Construction and Building Materials*, vol. 143, pp. 312–321, 2017.

[20] K. P. Zhou, R. G. Gao, and F. Gao, "Particle flow characteristics and transportation optimization of superfine unclassified backfilling," *Minerals*, vol. 7, no. 1, p. 6, 2017.

[21] C. H. Hou, Z. Q. Yang, Q. Gao, and D. X. Chen, "Experimental research on a new filling material compound of whole tailings and rod milling sand in Jinchuan mine," *Journal of Shandong University of Science and Technology*, vol. 34, no. 3, pp. 78–84, 2015.

[22] Y. J. Xu, K. P. Zhou, J. L. Li, and Y. M. Zhang, "Study of rock NMR experiment and damage mechanism analysis under freeze-thaw condition," *Rock and Soil Mechanics*, vol. 33, no. 10, pp. 3001–3005, 2012.

[23] J. Y. Jehng, *Microstructure of Wet Cement Pastes: a Nuclear Magnetic Resonance Study*, Ph.D. thesis, Northwestern University, Evanston, IL, USA, 1995.

[24] M. G. Prammer, E. D. Drack, J. C. Bouton et al., "Measurements of clay-bound water and total porosity by magnetic resonance logging," *Log Analyst*, vol. 37, no. 6, 1996.

[25] J. L. Shang, J. H. Hu, K. P. Zhou, X. W. Luo, and M. Aliyu, "Porosity increment and strength degradation of low-porosity sedimentary rocks under different loading conditions," *International Journal of Rock Mechanics and Mining Sciences*, vol. 75, pp. 216–223, 2015.

[26] Q. R. Xu, W. Y. Deng, B. Xu et al., "Quantitative analysis of soft clay three-dimensional porosity based on SEM image information," *Chinese Journal of Rock Mechanics and Engineering*, vol. 37, no. 7, pp. 1497–1502, 2015.

[27] R. G. Gao, K. P. Zhou, and J. L. Li, "Research of the mechanisms of backfill formation and damage," *Materiali in Tehnologije*, vol. 52, no. 2, pp. 163–169, 2018.

[28] P. J. M. Monteiro and P. K. Mehta, *Concrete: Microstructure, Properties and Materials*, Prentice-Hall, London, UK, 2006.

[29] A. A. Ramezanianpour, *Cement Replacement Materials: Properties, Durability, Sustainability*, Springer-Verlag, Berlin, Heidelberg, Germany, 2014.